



1 Water-soluble iron correlation to primary speciated organics in low-emitting vehicle exhaust

2 Joseph R. Salazar*, Benton T. Cartledge*, John P. Haynes*, Rachel York-Marini*, Allen L
3 Robinson‡, Greg T. Drozd[€], Allen H. Goldstein[¥], Sirine C. Fakra[€], Brian J. Majestic*

4 *University of Denver, Department of Chemistry and Biochemistry

5 ‡Carnegie Mellon University, College of Engineering

6 ¥University of California, Berkeley Department of Civil and Environmental Engineering

7 €Colby College Department of Chemistry

8 [€]Advanced Light Source, Lawrence Berkeley National Laboratory, Berkeley, CA 94720

9

10 *Correspondence to:* Brian J. Majestic (brian.majestic@du.edu)

11

12 **Abstract**

13

14 Iron is the most abundant transition element in airborne PM, primarily existing as Fe(II)
15 or Fe(III). Generally, the fraction of water-soluble iron is greater in urban areas compared to
16 areas dominated by crustal emissions. To better understand the origin of water-soluble iron in
17 urban areas, tail-pipe emission samples were collected from 32 vehicles with emission
18 certifications of Tier 0, low emission vehicles (LEV I), tier two low emission vehicles (LEV II),
19 ultralow emission vehicles (ULEV), superultra-low emission vehicles (SULEV), and partial-zero
20 emission vehicles (PZEV). Components quantified included gases, inorganic ions, EC/OC, total
21 metals and water-soluble metals. In addition, naphthalene and various classes of C12-C18
22 intermediate volatility organic compounds (IVOC) were quantified for a subset of vehicles:
23 aliphatic, single ring aromatic (SRA), and polar (material not classified as either aliphatic or
24 SRA). Iron solubility in the tested vehicles ranged from 0 – 82% (average = 30%). X-ray
25 absorption near edge structure (XANES) spectroscopy showed that Fe(III) was the primary
26 oxidation state in 14 of the 16 tested vehicles, confirming that the presence of Fe(II) was not the
27 main driver of water-soluble Fe. Correlation of water-soluble iron to sulfate was insignificant, as
28 was correlation to every chemical component, except to naphthalene and some C12- C18 IVOCs



29 with R^2 values as high as 0.56. A controlled benchtop study confirmed that naphthalene, alone,
30 increases iron solubility from soils by a factor of 5.5 and that oxidized naphthalene species are
31 created in the extract solution. These results suggest that the large driver in water-soluble iron
32 from primary vehicle tail-pipe emissions is related to the organic composition of the PM,
33 indicating the organic fraction of the PM influences the behavior and solubility of iron.

34 **1. Introduction**

35 Iron has been identified as a limiting nutrient for phytoplankton in approximately half of
36 the world's oceans, with deposition from the atmosphere as the major source (Moore and Abbott,
37 2002; Sholkovitz et al., 2012). Phytoplankton is one of the controlling factors of fixed nitrogen in
38 many parts of the oceans and, consequently, plays a major role in the ocean's biogeochemical
39 cycles (Baker et al., 2006; Chen and Siefert, 2004; Kraemer, 2004; Shi et al., 2012; Tagliabue et
40 al., 2017). Also, water-soluble iron fractions are linked to the creation of reactive oxygen species
41 (ROS) in lung fluid and in environmental matrices through Fenton chemistry (Hamad et al.,
42 2016). These ROS impart oxidative stress on the respiratory system, contributing to various
43 health effects (Landreman et al., 2008; Park et al., 2006; Verma et al., 2014).

44 Annually, approximately 55 Tg of iron enters the atmosphere from crustal sources (Luo
45 et al., 2008). Of this, 14-16 Tg are deposited into the ocean, impacting the marine life and
46 influencing the ecosystems (Gao, 2003; Jickells et al., 2005). Typically, airborne iron from
47 crustal sources ranges from 0.05-2% water-soluble of the total iron (Bonnet, 2004; Sholkovitz et
48 al., 2012). Relative water-soluble iron in urban environments is higher, ranging from 2-50% of
49 the total (Majestic et al., 2007; Sedwick et al., 2007; Sholkovitz et al., 2012). It is suggested that
50 combustion sources including fossil fuel burning, incinerator use and biomass burning may be a
51 large contributor to the water-soluble iron fraction, contributing $0.66\text{-}1.07\text{ Tg a}^{-1}$ of water-soluble



52 iron and this iron has been correlated to anthropogenic sources (Chuang et al., 2005; Luo et al.,
53 2008; Sholkovitz et al., 2009). Even though total iron emissions from combustion sources are
54 small in comparison to crustal sources, the relative insolubility of crustal iron leads to the
55 possibility that combustion sources contribute 20%-100% of water-soluble iron into the
56 atmosphere (Luo et al., 2008; Sholkovitz et al., 2012).

57 Previous studies in tunnels and parking structures have reported iron ranging from five to
58 approximately $3,500 \text{ ng m}^{-3}$, revealing that brake wear, tire wear, resuspended road dust, and tail
59 pipe emissions can be important sources of trace elements (Kuang et al., 2017; Lawrence et al.,
60 2013; Li and Xiang, 2013; Lough et al., 2005; Park et al., 2006; Verma et al., 2014). Within the
61 engine, iron is likely to result from combusted gasoline, which has pre-combusted concentrations
62 ranging from $13\text{-}1000 \mu\text{g L}^{-1}$ (Lee and Von Lehmden, 1973; Santos et al., 2011; Teixeira et al.,
63 2007). Additionally, computational models of combustion in engines suggest that iron emissions
64 could originate from the fuel injector nozzle inside the engine block (Liati et al., 2015).

65 There are many different factors that may contribute to water-soluble iron and, as a result,
66 several different hypotheses have been developed relating to how iron is solubilized in ambient
67 atmospheres. First, correlation of ambient iron to sulfates in ambient aerosols suggest the
68 possibility of iron solubilization (Desboeufs et al., 1999; Hand et al., 2004; Mackie et al., 2005;
69 Oakes et al., 2012b). However, laboratory studies investigating the heterogeneous chemistry of
70 iron have not shown any change in iron water-solubility, speciation, or oxidation state upon
71 exposure to gaseous SO_2 (Cartledge et al., 2015; Luo et al., 2005; Majestic et al., 2007; Oakes et
72 al., 2012a). A second hypothesis is that particle-bound iron oxidation state may control iron
73 water solubility. Thus far, the limited field studies have been unable to show that iron oxidation
74 state is correlated to iron's resulting water solubility, as the majority of iron found in aerosol



75 particles is in the less soluble Fe(III) oxidation state (Luo et al., 2005; Majestic et al., 2007;
76 Oakes et al., 2012a). A third, broad, iron solubilization hypothesis emphasizes an iron-organic
77 interaction (Baba et al., 2015; Vile et al., 1987). For example, a significant increase in water-
78 soluble iron is observed in the presence of oxalate and formate in ambient aerosols and in cloud
79 droplets (Paris et al., 2011; Zhu et al., 1993). Other studies have suggested that the photolysis of
80 polycyclic aromatic hydrocarbons leads to reduced iron, which may result in greater iron water
81 solubility (Faiola et al., 2011; Haynes et al., 2019; Pehkonen et al., 1993; Zhu et al., 1993).

82 In this study, we explore all three hypotheses (bulk ions, iron oxidation state, and organic
83 speciation) in relation to iron solubility. Specifically, we examine the water-soluble iron emitted
84 from 32 light duty gasoline vehicles with certifications of Tier 0, low emission vehicle (LEV I),
85 tier two low emission vehicles (LEV II), ultralow emission vehicles (ULEV), superultra-low
86 emission vehicles (SULEV), and partial-zero emission vehicles (PZEV). The total and water-
87 soluble trace elements are compared to the ions, gaseous compounds, and organic emissions
88 from the same vehicle set. Additionally, we acquired data on the emitted iron oxidation states on
89 the exhaust particles. From this data set, real tail-pipe emission samples were explored to
90 discover how various components of automobile exhaust affect the water solubility of iron.

91 **2. Materials and Methods**

92 **2.1. Sample Collection**

93 Exhaust samples from 32 gasoline vehicles were collected at the California Air Resources
94 Board (CARB) Haagen-Smit laboratory over a six-week period. Standard emission test results
95 from this campaign have been reported previously (Saliba et al., 2017). A description of the
96 dynamometer, emission dilution system, and instrumentation used in the vehicle set up is
97 provided elsewhere (May et al., 2014; Saliba et al., 2017). Briefly, each vehicle was tested on a



98 dynamometer using the cold-start Unified California (UC) Drive Cycle or the hot start Modal
99 Arterial Cycle 4. Emission samples were collected using a constant volume sampler from which
100 a slipstream of dilute exhaust was drawn at a flow rate of 47 L min^{-1} . The particulate exhaust
101 emissions were then collected on the pre-cleaned Teflon filters. The Teflon filters were stored in
102 a freezer until extraction and analysis was performed. Filter holders were maintained at 47°C
103 during sampling as per the CFR86 protocol.

104 The vehicles were recruited from private citizens, rental car agencies, or part of the Air
105 Resource Board fleet. The vehicles tested were categorized by model years (1990-2014), vehicle
106 type (passenger car and light-duty trucks), engine technologies (GDI and PFI), emission
107 certification standers (Tier1 to SULEV), make, and model. All vehicles were tested using the
108 same commercial gasoline fuel which had a 10 % ethanol blend and a carbon fraction of 0.82
109 (Saliba et al., 2017).

110 Gases (CO , CO_2 , CH_4 , NO , and NO_2) and total hydrocarbons (THC) were collected into
111 heated Tedlar bags by UC Drive Cycles. Analysis of CO and CO_2 was measured by
112 nondispersive infrared detectors (IRD-4000), CH_4 by gas chromatography-FID, NO_x by
113 chemiluminescence (CLD 4000) and THC by FID (Drozd et al., 2016; Saliba et al., 2017).
114 Particle phase emissions were collected using three sampling trains operated in parallel off of the
115 end of the CVS dilution tunnel. Train 1 contained a Teflon filter (47 mm, Pall-Gelman, Teflo
116 R2PJ047). Train 2 contained two quartz filters (47 mm, Pall-Gelman, Tissuquartz 2500 QA0UP)
117 in series. Train 3 contained an acid-cleaned Teflon filter followed by a quartz filter (47 mm,
118 Teflo, Pall Life Sciences, Ann Arbor, MI). The Teflon filter in Train 1 was analyzed by ion
119 chromatography for water-soluble anions and cations and these data are presented elsewhere
120 (Hickox et al., 2000). Train 2 included two parallel sets of Tenax-TA sorbent tubes (Gerstel)



121 downstream of the Teflon filter. The first set was 2 tubes connected in parallel. One of these
122 tubes was used to collect emissions during the cold start phase of UC (the first five minutes,
123 commonly referred to as bag 1). The other tube was used to sample emissions during the
124 combined hot-running and hot start phases of the UC (bags 1 and 2). The second set of sorbent
125 tubes was connected in series to collect emissions over the entire UC test. The flow rate was 0.5
126 L min⁻¹ through each Tenax tube. The Teflo filter in Train 3 was used for total and water-soluble
127 trace element analysis and particle-bound iron oxidation state and is the focus of this study.

128 **2.2. Materials Preparation**

129 All vessel cleaning and analytical preparation for the trace elements was performed under
130 a laminar flow hood with incoming air passing through a high efficiency particulate air (HEPA)
131 filter. All water used was purified to 18.2 MΩ-cm (Milli-Q Thermo-Fisher Nanopore). Fifteen
132 and 50 mL plastic centrifuge vials, Petri dishes (Fisher), Teflon forceps (Fisher), syringe
133 (Fisher), nitro cellulose paper (Fisher), and syringe cases (Life Sciences Products) were prepped
134 by an acid cleaning process. For the plastic centrifuge vials, Petri dishes, Teflon forceps, syringe,
135 and syringe cases this involved 24-hour soaks in a 10% reagent grade nitric acid bath followed
136 by 10% reagent grade hydrochloric bath then a 3% trace metal grade nitric acid (Fisher) resting
137 bath with MQ rinses before, after and between each step. The nitro cellulose paper was cleaned
138 by soaking in 2% HCl for 24 hours then rinsing with MQ water. Then, 2% HCl and MQ water
139 were pushed through the filter. Teflon beaker liners were cleaned by an acetone rinse, then an
140 overnight bath of 100% HPLC-grade acetonitrile and a final overnight bath of 5% trace-metal
141 grade nitric acid. 0.20 micron syringe filters (Whatman, Marlborough, MA) were prepared with
142 10% trace-metal grade hydrochloric acid, MQ water and 5% nitric acid rinse. All materials were



143 handled with powder free nitrile gloves (Fisher), double bagged, and handled inside a
144 polypropylene laminar flow hood (NuAire, Plymouth, MN).

145 The 47 mm Teflon filters were cleaned by submerging them in 10% trace metal grade
146 nitric acid and rinsing with MQ water. The filters were then stored in the acid cleaned Petri
147 dishes and sealed with Teflon tape for storage.

148 **2.3. Water-soluble metals sample preparations**

149 Water-soluble elements were extracted for 2 hours from the Teflon filter on a shaker table
150 in 10 mL of MQ water. The water extract was filtered with 2 μm pore size nitro cellulose filters.
151 The Teflon filter and the nitro cellulose filters were saved for total metals digestion. The water-
152 soluble element extract was acidified to 5% trace-metal grade nitric acid and 2.5% trace-metal
153 grade hydrochloric acid to be analyzed by inductively coupled plasma mass spectrometry (ICP-
154 MS, Agilent 7700).

155 **2.4. Sample preparation for total elemental analysis**

156 After the polymethylpentene ring was removed from the Teflon filters and ~3%
157 (measured exactly) of the filters cut and saved for X-ray absorption near edge structure
158 (XANES) spectroscopy, the Teflon and the nitro cellulose filters for each sample were placed
159 together into a microwave digestion vessel. To each digestion vessel, 750 μL of concentrated
160 trace metal grade nitric acid, 250 μL of concentrated trace grade hydrochloric acid, 100 μL of
161 concentrated trace grade hydrofluoric acid, and 100 μL of 30% hydrogen peroxide was added.
162 These samples were digested (Ethos EZ, Milestone Inc) according to the following a temperature
163 program: 15-minute ramp to 200 °C, then held at 200 °C for 15 minutes, and a 60-minute cooling



164 period.(Cartledge and Majestic, 2015) The samples were cooled to room temperature for 1 hour
165 and the solution was diluted to 15 mL with MQ water and analyzed via ICP-MS.

166 **2.5. Elemental analysis**

167 Blank filters and standard reference materials (SRMs) were digested alongside the
168 exhaust samples using the same digestion process described above. Three SRMs were used to
169 address the recoveries of our digestion process: urban particulate matter (1648a, NIST), San
170 Joaquin Soil (2709a, NIST), and Recycled Auto Catalyst (2556, NIST). The recoveries of the
171 SRMs were between 80-120%. The elements analyzed included Na, Mg, Al, K, Ca, Ti, V, Cr,
172 Mn, Fe, Co, Ni, Cu, Zn, As, Se, Rb, Sr, Mo, Rh, Pd, Ag, Cd, Sb, Cs, Ba, Ce, Pt, Pb, U. Indium
173 (~1 ppb) was used as an internal standard and a He collision cell was used to remove isobaric
174 interferences.

175 **2.6. XANES Spectroscopy**

176 X-ray absorption near-edge structure (XANES) and X-ray fluorescence (XRF) data for
177 16 vehicle exhaust samples were collected at the Advanced Light Source Microprobe beamline
178 (10.3.2), Lawrence Berkeley National Laboratory, Berkeley, CA (Marcus et al., 2004). To locate
179 iron spots on the filters, a broad XRF elemental map of each sample was acquired at 10 keV
180 using 12 μm by 12 μm pixel size and 50 ms dwell time per pixel. μXRF spectra were
181 simultaneously recorded on each pixel of the map. Iron oxidation state and iron-bearing phases
182 were investigated using iron K-edge extended XANES. The spectra were recorded in
183 fluorescence mode by continuously scanning the Si (111) monochromator (Quick XAS mode)
184 from 7011 to 7415 eV. The data were calibrated using an iron foil with first derivative set at
185 7110.75 eV (Kraft et al., 1996). All data were recorded using a seven-element solid state Ge



186 detector (Canberra, ON). The spectra were deadtime corrected, deglitched, calibrated, pre-edge
187 background subtracted and post-edge normalized using a suite of LabVIEW custom programs
188 available at the beamline (Marcus et al., 2008). To rapidly survey iron oxidation state, a valence
189 scatter plot was generated from normalized XANES data using a custom Matlab code and a large
190 database of iron standards (10.3.2 XAS database) (Marcus et al., 2008). Least-square linear
191 combination fitting (LCF) was subsequently performed in the range 7090 to 7365 eV to confirm
192 iron valence and further identify the major mineral groups present. The best fit was chosen based
193 on 1) minimum normalized sum-square value ($NSS=100 \times [\sum(\mu_{\text{exp}} - \mu_{\text{fit}})^2 / \sum(\mu_{\text{exp}})^2]$), where the
194 addition of a spectral component to the fit required a 10% or greater improvement in the NSS
195 value, and 2) on the elements detected in the μ XRF spectrum recorded on each XANES spot.
196 The uncertainty on the percentages of species present is estimated to be $\pm 10\%$.

197 **2.7. Organic Speciation**

198 A subset (10) of the 32 samples were quantified for IVOC using electron impact ionization
199 with methods similar to that of Zhao et al., except adapted for GCxGC methods (Zhao et al.,
200 2015, 2016). IVOC material was classified into three categories: aliphatic, single ring aromatic
201 (SRA), and polar (Drozd et al., 2019). Classification within these three classes of compounds
202 was determined by differences in second dimension retention time (polarity space) and by mass
203 spectral characteristics in our GCxGC-MS analysis. All three classes of compounds were
204 quantified by either compound specific calibration using known standards or relating total ion
205 chromatogram (TIC) signals to calibration standards of similar volatility and polarity. In
206 GCxGC, the TIC signal corresponds to a blob, or a region in volatility and polarity retention
207 space. The GC-Image software package was used to create blobs from 2D chromatograms.
208 Compounds were quantified by relating their TIC signal to that of the nearest standard in terms



209 of polarity and volatility. Volatility bins were defined that are evenly spaced with their center
210 elution times corresponding to each *n*-alkane. TIC blobs were quantified using the calibration for
211 the available standard of similar polarity in the same volatility bin.

212 **2.8. Emission Factor Calculations**

213 Emissions data are presented as fuel-based emission factors (EF). Emission factors are
214 calculated as the amount of analyte emitted by mass per gram of fuel emitted.

$$215 \quad EF_i(g\ g - fuel^{-1}) = \Delta m_i \frac{x_c(g)}{\Delta CO_2(g) + \Delta CO(g) + \Delta THC(g)}$$

216 ΔCO_2 , ΔCO , and ΔTHC are the background corrected carbon concentration of CO_2 , CO , and
217 THC (Drozd et al., 2016; Goldstein et al., 2017), respectively. x_c is the fuel carbon mass
218 fraction of 0.82. Δm_i is the blank subtracted concentrations of species *i*.

219 **2.9. Naphthalene and Iron Benchtop Study**

220 To better understand the production of soluble iron during the water extraction process, a
221 bench-top study was performed using three varying forms of iron with naphthalene. The iron
222 stock solutions/suspensions included: 1) standardized San Joaquin soil (NIST SRM 2709a)
223 containing 25 ppm total iron (soluble + insoluble) iron to determine the effects of crustal iron, 2)
224 iron(II) sulfate to a concentration of 25 ppm to examine the effect of a soluble iron(II) source,
225 and 3) iron(III) sulfate to examine a source of soluble iron(III). In parallel, 100 mg of
226 naphthalene crystals were added to 200 mL of MQ water. For the experiment, 100 mL of the
227 naphthalene suspension and 1 mL of the iron suspension were added to Teflon liners (250 ppb
228 iron total), which were inserted into a jacked glass beaker temperature controlled to 25 °C. After
229 16 hr of stirring, 2 ml were filtered (0.2 μm) and acidified to 5% nitric acid. Soluble iron released



230 from the soil both in the presence and absence of naphthalene was analyzed by ICP-MS.
231 Chemical changes in naphthalene in the presence and absence of iron were monitored by HPLC.

232 **3. Results and Discussion**

233 *3.1. Total and water-soluble element exhaust concentrations*

234 **Table 1:**

235 Emissions of ions, organic species, gaseous species, and EC/OC from these tests have
236 been published previously (Drozd et al., 2016, 2019; Goldstein et al., 2017; Saliba et al., 2017).
237 In order to obtain a better understanding of the factors that influence iron solubility, we compare
238 these with the total elements, trace elements, and iron oxidation state measurements. Generally,
239 the elements with the highest EF are the lighter crustal elements Ca, Al, and Fe, with average EF
240 200, 100, and 80 $\mu\text{g kg-fuel}^{-1}$ (Table 1), respectively. Iron has the third highest average EF of all
241 the elements and the highest of all transition elements, ranging from 0 – 200 $\mu\text{g Fe kg-fuel}^{-1}$.
242 This is followed by three first row transition elements: Zn, Cu, and Ni with the respective
243 average EF of 60, 20, and 5 $\mu\text{g kg-fuel}^{-1}$. Other notable elements include Rh, Pd and Pt, likely
244 originating from the catalytic convertor, with the respective average EF of 0.05, 0.7, and 0.04 μg
245 kg-fuel^{-1} . Toxic elements include Cr, Pb, Mo and Sb with respective EF 5, 0.8, 5 and 0.2 $\mu\text{g kg-}$
246 fuel^{-1} . A previous study has shown that various elements are enriched in used motor oil such as
247 copper, zinc, manganese, iron and lead which could originate from engine wear (Majestic et al.,
248 2009).

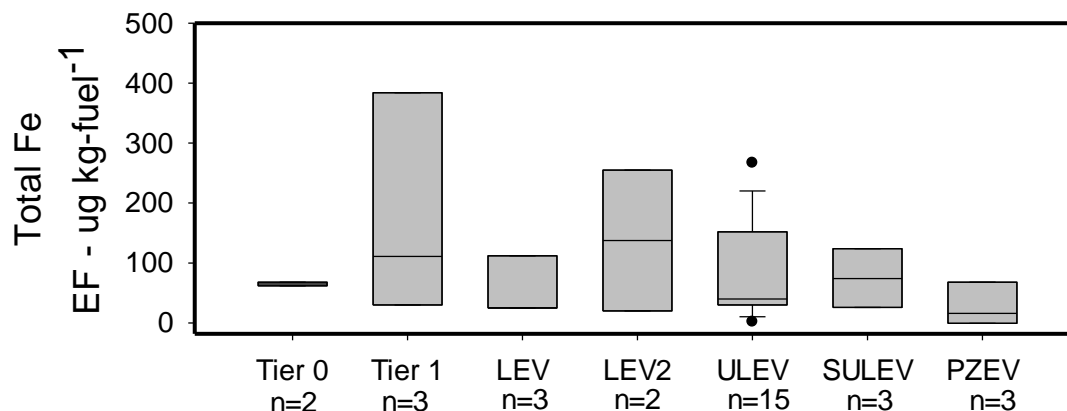
249 Table 1 also shows the EF for the water-soluble fraction of the trace elements. The water-
250 soluble EF for iron ranges from 0-150 $\mu\text{g kg-fuel}^{-1}$; or 0-82% of the total. At 20 $\mu\text{g kg-fuel}^{-1}$,
251 average water-soluble iron was the third largest EF of all elements. There were relatively high



252 emissions of a few other water-soluble elements such as Ca with an average EF of $200 \mu\text{g kg}^{-1}$
253 fuel^{-1} and Zn with tailpipe emissions averaging $40 \mu\text{g kg-fuel}^{-1}$.

254 **Table 2:**

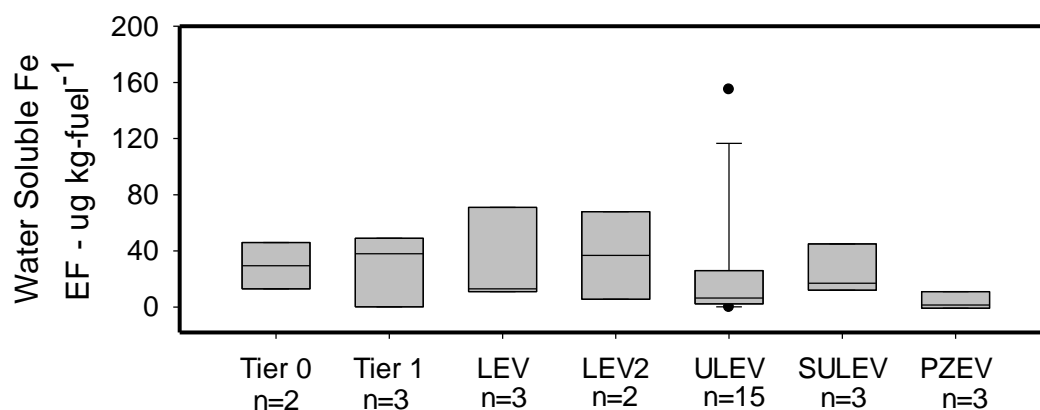
255 Only a few studies report tailpipe emissions (i.e., dynamometer testing) of trace elements
256 for diesel and gasoline-powered passenger cars and even fewer which have reported iron water
257 solubility in low emitting vehicles (Tier1 to SULEV) (Norbeck et al., 1998; Schauer et al., 2002).
258 Table 2 compares the average exhaust PM composition and trace elements km^{-1} in this study to
259 literature values for other passenger vehicles, including one diesel and three gasoline exhaust
260 studies. For all elements, the per km emissions were greater in the diesel cohort, relative to the
261 gasoline vehicles. Compared to previous studies, the trace elements emitted from older gasoline
262 passenger vehicles resulted in an order of magnitude higher emissions for all elements, except
263 for aluminum, which only showed a factor of ~ 2 increase in older vehicles (Table 2). Iron shows
264 a large range in the three studies of gasoline vehicles, ranging from $8.3\text{--}280 \mu\text{g km}^{-1}$, compared
265 to the $0\text{--}62 \mu\text{g km}^{-1}$ measured in this study.



266



267 Figure 1: Total iron from the 32 vehicles tested reported in EF ($\mu\text{g kg-fuel}^{-1}$). The center black
268 line represents the median value and the edges of the boxes represent the 25th and 75th percentiles
269 while the whiskers extent are the 10th and 90th percentiles.



270

271 Figure 2: Water-soluble iron from the 32 vehicles tested reported in EF ($\mu\text{g kg-fuel}^{-1}$). The center
272 black line represents the median value and the edges of the boxes represent the 25th and 75th
273 percentiles while the whiskers are the 10th and 90th percentiles.

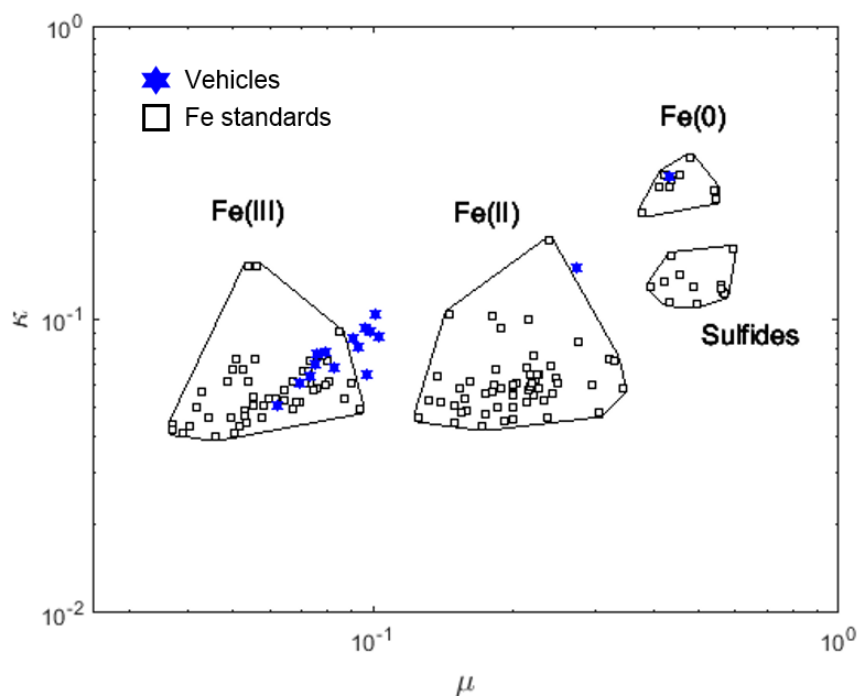
274

275 The large ranges in iron solubility of the previous studies led us to explore and compare
276 the newer emission certification standard (Figure 1 and 2). Total iron did not trend strongly with
277 emission certification standard, although, on average, total iron is less in the Tier 0 and LEV
278 vehicles. Water-soluble iron shows a small average decrease of approximately $5 \mu\text{g kg-fuel}^{-1}$
279 between ULEV and SULEV vehicles, and a further average decrease for the PZEV vehicles of
280 $3.9 \mu\text{g kg-fuel}^{-1}$.

281 *3.2. Iron correlations with bulk exhaust components and iron oxidation state*



282 To explore what factors and if any exhaust components are associated with the presence
283 of water-soluble iron, linear regression analyses were used to compare soluble iron to different
284 chemical species in the exhaust. Solubility from the direct exhaust was explored by comparing
285 the EFs of both sulfate and nitrate to iron, and water-soluble iron was not correlated to either of
286 these species (SI1). The EFs for water-soluble iron and CO₂ showed no correlation, suggesting
287 that overall fuel use was not an important factor for water-soluble iron production (SI1). Total
288 iron was correlated to the water-soluble iron indicating the total amount of iron may have an
289 impact on soluble iron (SI2). Finally, to evaluate if water-soluble iron and overall particulate
290 carbon relate, the EFs for elemental carbon (EC) and organic carbon (OC) were compared to that
291 of soluble iron and, again, no correlation was observed (SI1).



292



293 Figure 3: Fe valence scatter plot generated from Fe K-edge XANES data where κ and μ are
294 normalized absorbance values at 7113 eV and 7117.5 eV respectively. Empty black squares
295 represent Fe standards of known valence while blue-filled stars represent vehicle exhaust
296 samples.

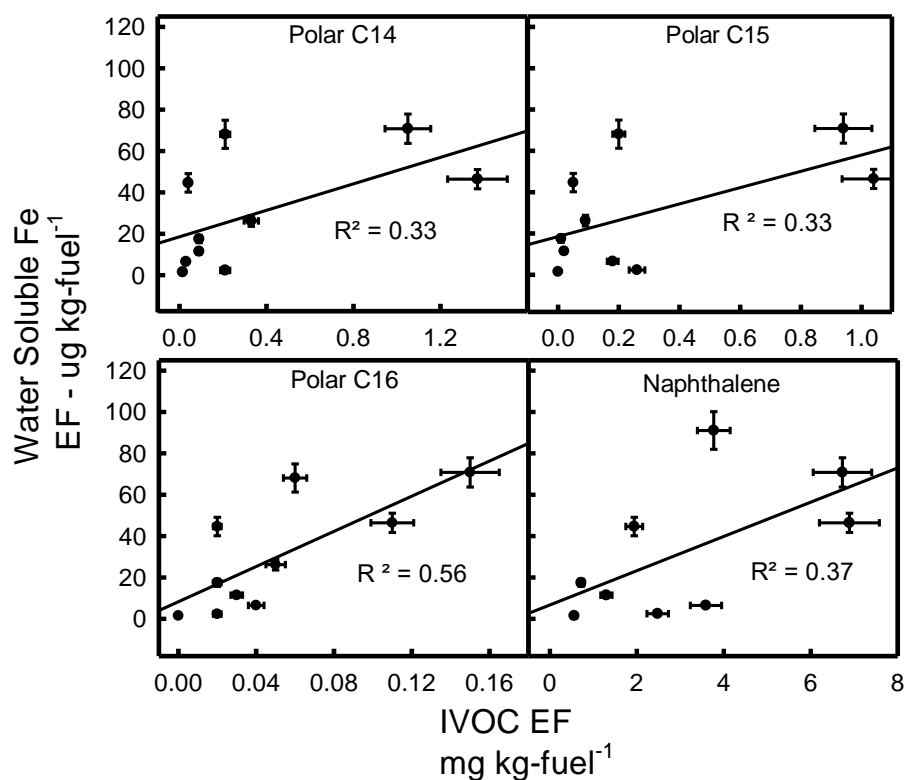
297

298 As no correlation between water-soluble iron and bulk chemical species was observed
299 (SI1 and SI3), the importance of the particle-bound iron oxidation state was investigated. Since
300 Fe(II) is known to be more soluble than Fe(III), the expectation was that exhaust samples having
301 a large Fe(II) character would have a greater iron solubility, relative to those containing Fe(III)
302 or to Fe(0) (Stumm and Morgan, 1996). Figure 3 presents a scatter plot of the iron valence in 16
303 of the exhaust samples, compared with iron-bearing standards of known valence. This valence
304 plot is generated from iron K-edge XANES data where parameters κ and μ are defined as
305 normalized absorbance values at 7113 eV and 7117.5 eV, respectively. We observe that the
306 exhaust-iron is primarily in the Fe(III) oxidation state, except for two vehicles: sample 11,
307 dominated by Fe(0) and sample 15, containing a combination of Fe(0) and Fe(III) (SI4). Sample
308 11 is an extreme case, having 0 % iron solubility and highly elevated amount of EC at 305 μg
309 kg-fuel^{-1} (study average = 78 $\mu\text{g kg-Fuel}^{-1}$). The presence of Fe(0) is consistent with high EC, as
310 both observations suggest a lack of oxidation during the combustion and emission process.
311 While the valence plot (Figure 3) put sample 15 as mostly Fe(II), the LCF actually showed that it
312 was a mixture of Fe(0) and Fe(III). And, this sample contained only 10% water-soluble iron, less
313 than the cohort average. The study-wide solid phase iron oxidation state is primarily Fe(III) or
314 mixed oxidation state (Fe(III) and Fe(0)) (see Figure 3), averaging about 30% water-soluble iron,
315 well above the crustal background.



316 LCF XANES fitting (SI4) showed Fe(III) oxides and oxyhydroxides as the dominant group,
317 followed by Fe(III) sulfates and iron silicates (SI4). Hematite (α -Fe₂O₃) and maghemite (γ -
318 Fe₂O₃) were the most consistently detected Fe(III) oxides. Iron was detected in all samples, with
319 Zn, Cr and Cu the main other elements detected in nearly all samples (detection of low-Z
320 elements below sulfur or high-Z elements above zinc was not possible in our experimental
321 conditions). Overall, these results strongly suggest that the main driver of water-soluble iron is
322 not associated with the particle-bound iron oxidation state. Further investigation for the LCF
323 XANES fitting showed that 34% of iron speciated was Fe(III)-oxyhydroxides associated with
324 organic material, leading to the investigation of longer chain IVOC and naphthalene (SI6).

325 3.3. Iron solubility and speciated organics



326

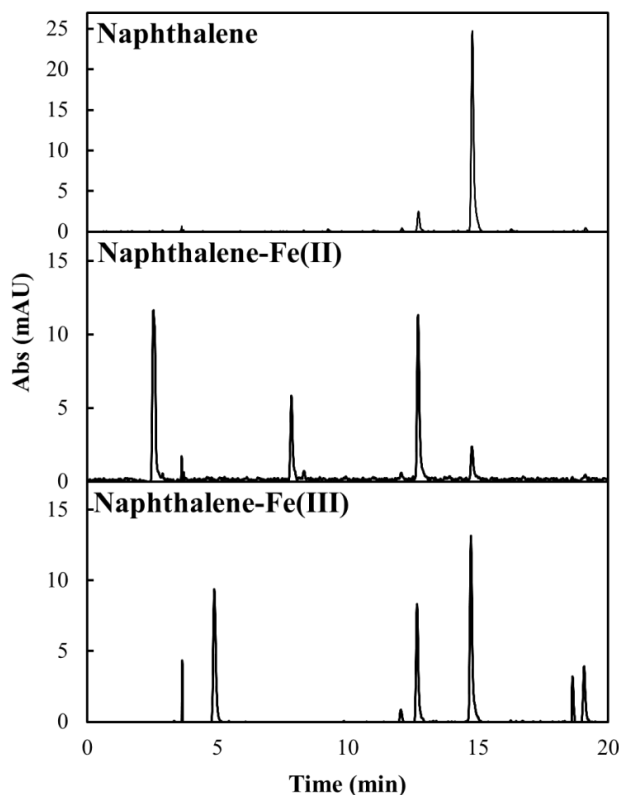


327 Figure 4: Scatter plots of water-soluble iron versus the sum of IVOCs reported in EF (g kg⁻¹-
328 ¹).

329

330 Finally, the relationship between water-soluble iron and speciated organics, specifically
331 naphthalene and IVOCs, was examined. In contrast with all other measured parameters, Figure 4
332 shows relatively strong correlations between water-soluble iron and some of the IVOC species.
333 Figure 4 presents the classifications which have the strongest correlation with water-soluble iron.
334 Water-soluble iron relationships with other IVOCs can be found in the supplementary
335 information (SI8). The correlation to water-soluble iron is highest for IVOC-polar species with
336 16 carbons ($R^2 = 0.56$).

337 As water-soluble iron trends well with naphthalene and polar-IVOCs, but not with bulk
338 EC or OC, it is highly suggestive that iron solubility from the direct emission samples is
339 primarily dependent on interactions with the species of carbon present in the particles during the
340 extraction process. To better understand these interactions, a preliminary laboratory study was
341 conducted to explore both i) the effect of these organic compounds on iron solubility and ii) the
342 effect of soluble iron on the oxidation of organic compounds during the extraction process.
343 Specifically, when naphthalene was added to an insoluble iron source (a soil), iron solubility
344 increased from 0.8 to 4.2 % of the total, or by a factor of ~5.5, showing that the addition of
345 naphthalene, alone, can have a significant effect on iron water solubility and that this effect
346 likely is important during the extraction process.



347

348 Figure 5: HPLC of resulting reaction between naphthalene and water-soluble iron. Phthalic acid
349 at 12.5 minutes, phthalic anhydride at 7.5 minutes, naphthol at 15 minutes and naphthalene at 20
350 minutes. The column uses a C18 stationary phase on beads with 80Å pore size.

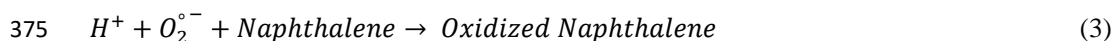
351 Lacking oxidized functional groups, naphthalene was not expected to chelate iron or to,
352 otherwise, have the ability to increase iron solubility. Thus, we investigated what compounds are
353 formed from naphthalene during these extractions. Figure 5 shows the new oxidized products
354 formed from naphthalene during the water extraction. In the presence of soluble iron, HPLC
355 retention time analysis shows the presence of phthalic acid (12.5 minutes), phthalic anhydride
356 (7.5 minutes), and naphthol (15 minutes). The peaks at and below 5 min were not identified but,



357 based on the retention times, these are thought to be low molecular mass, highly polar organic
358 products and is consistent with other studies (Haynes et al., 2019)

359 3.4. Iron-carbon interactions

360 There are at least two methods in which organic compounds can lead to increased iron
361 solubility: a) reduction of Fe(III) to Fe(II) or b) bringing soluble iron into solution via chelation.
362 The first one is generally achieved by photochemistry (Pehkonen et al., 1993), which is not
363 directly applicable to this study. The second, chelation, generally requires oxidized functional
364 groups as shown in Figure 5. The extent of the ability for phthalic acid (a dicarboxylic acid) to
365 chelate iron has not been reported, however, it is known that similar molecular mass organic
366 diacids have significant ability to chelate iron, thus pulling it into solution (Paris and Desboeufs,
367 2013). Here, we suggest that the observed correlations between IVOC/naphthalene and water-
368 soluble iron can be best explained with Fenton reactions, resulting in propagation of radical
369 reactions (Pehkonen et al., 1993). As shown from the Fe XANES valance plot, the iron is
370 predominately Fe(III) (Figure 4). In addition to the Fe(III), it has been shown that H₂O₂ forms in
371 PM_{2.5} water extracts and it been speculated that this formation is from various transition metals
372 and/or quinones found in PM_{2.5} (Wang et al., 2012).



376

377 In the presence of H₂O₂, Fe(III) is known to undergo reaction (1) (Neyens and Baeyens,
378 2003; Pignatello et al., 2006), resulting in the formation of Fe(II) and HO₂ (Pignatello et al.,
379 2006; Rubio-Clemente et al., 2014), which degrades into superoxide, O₂⁻, and H⁺ (2). Superoxide
380 has the ability to oxidize organic compounds, particularly aromatic structures (3) (Lair et al.,



381 2008). The resulting structures of these oxidized compounds typically have two oxygen atoms,
382 which could be arranged in various functional groups (Lair et al., 2008; Rubio-Clemente et al.,
383 2014), also observed from the HPLC chromatograms. Oxidized single ring aromatic structures
384 have a strong affinity to iron and have the ability chelate iron into aqueous solution (Hosseini
385 and Madarshahian, 2009). Based on the laboratory studies of naphthalene and soluble-iron
386 presented here, naphthalene and/or IVOC oxidation during the extraction process is the most
387 likely path towards increased iron solubility in primary tailpipe emissions.

388 **4. Conclusions**

389 This study shows water-soluble iron is directly formed from vehicle exhaust. The results
390 show that iron is solubilized in water by specific organic compounds present in automobile
391 exhaust, and that soluble iron is not necessarily dictated by the overall OC content. Thus, the
392 implication is that anthropogenic water-soluble iron is a result of chelation from specific organic
393 compounds, likely their eventual aqueous reaction products. Although the mechanism of these
394 aqueous transformations were not directly measured in this study, based on Fenton chemistry,
395 the primary compounds are expected to be oxidized versions of naphthalene and/or IVOCs
396 (Ledakowicz et al., 1999). Since these oxidation reactions occur fairly quickly (i.e., during the
397 water extraction), further studies are of interest to better understand how these organic
398 compounds interact with iron as it enters atmospheric waters and, also, the photo-chemical
399 interactions between iron and organics.

400

401

402



403 **Acknowledgements**

404 The authors thank the excellent and dedicated personnel at the California Air Resources
405 Board, especially at the Haagen–Smit Laboratory This study was funded by National Science
406 Foundation grant number 1342599. This research used resources of the Advanced Light Source,
407 which is a DOE Office of Science User Facility under contract no. DE-AC02-05CH11231.
408 Financial support was provided by the California Air Resources Board (Contract #12-318). The
409 California Air Resources Board also provided substantial in-kind support for vehicle
410 procurement, testing, and emissions characterization.

411 **Author contribution**

412 The sample collection scheme was designed by Allen L. Robinson, Allen H. Goldstein
413 and Brian J. Majestic. Samples were collected by Benton T. Cartledge and Greg T. Drozd.
414 Organic speciation was performed by Greg T. Drozd. Trace elements were quantified by Joseph
415 R. Salazar. Iron speciation was performed by Joseph R. Salazar, Rachel York-Marini and Brian
416 J. Majestic, with the interpretation effort led by Sirine C. Fakra. Bench-top naphthene
417 experiments were performed by John P. Haynes. Data integration was performed by Joseph R.
418 Salazar. The manuscript was prepared by Joseph R. Salazar and Brian J. Majestic.

419

420

421

422

423



424 **References**

- 425 Baba, Y., Yatagai, T., Harada, T. and Kawase, Y.: Hydroxyl radical generation in the photo-
426 fenton process: Effects of carboxylic acids on iron redox cycling, *Chem. Eng. J.*, 277, 229–241,
427 doi:10.1016/j.cej.2015.04.103, 2015.
- 428 Baker, A. R., Jickells, T. D., Witt, M. and Linge, K. L.: Trends in the solubility of iron,
429 aluminium, manganese and phosphorus in aerosol collected over the Atlantic Ocean, *Mar.*
430 *Chem.*, 98(1), 43–58, doi:10.1016/j.marchem.2005.06.004, 2006.
- 431 Bonnet, S.: Dissolution of atmospheric iron in seawater, *Geophys. Res. Lett.*, 31(3), L03303,
432 doi:10.1029/2003GL018423, 2004.
- 433 Cartledge, B. T. and Majestic, B. J.: Metal concentrations and soluble iron speciation, *Atmos.*
434 *Pollut. Res.*, (6), 495–505, 2015.
- 435 Cartledge, B. T., Marcotte, A. R., Herckes, P., Anbar, A. D. and Majestic, B. J.: The Impact of
436 Particle Size, Relative Humidity, and Sulfur Dioxide on Iron Solubility in Simulated
437 Atmospheric Marine Aerosols, *Environ. Sci. Technol.*, 49(12), 7179–7187,
438 doi:10.1021/acs.est.5b02452, 2015.
- 439 Chen, Y. and Siefert, R. L.: Seasonal and spatial distributions and dry deposition fluxes of
440 atmospheric total and labile iron over the tropical and subtropical North Atlantic Ocean, *J.*
441 *Geophys. Res. D Atmos.*, 109(9), doi:10.1029/2003JD003958, 2004.
- 442 Chuang, P. Y., Duvall, R. M., Shafer, M. M. and Schauer, J. J.: The origin of water soluble
443 particulate iron in the Asian atmospheric outflow, *Geophys. Res. Lett.*, 32(7), 1–4,
444 doi:10.1029/2004GL021946, 2005.



- 445 Desboeufs, K. V, Losno, R. and Cholbi, S.: The pH-dependent dissolution of wind-transported, ,
446 104, 1999.
- 447 Drozd, G. T., Zhao, Y., Saliba, G., Frodin, B., Maddox, C., Weber, R. J., Chang, M. C. O.,
448 Maldonado, H., Sardar, S., Robinson, A. L. and Goldstein, A. H.: Time Resolved Measurements
449 of Speciated Tailpipe Emissions from Motor Vehicles: Trends with Emission Control
450 Technology, Cold Start Effects, and Speciation, *Environ. Sci. Technol.*, 50(24), 13592–13599,
451 doi:10.1021/acs.est.6b04513, 2016.
- 452 Drozd, G. T., Zhao, Y., Saliba, G., Frodie, B., Maddox, C., Chang, M.-C. O., Maldonado, H.,
453 Sardar, S., Weber, R. J., Robinson, A. L. and Goldstein, A. H.: Detailed Speciation of
454 Intermediate Volatility and Semivolatile Organic Compound Emissions from Gasoline Vehicles:
455 Effects of Cold-Starts and Implications for Secondary Organic Aerosol Formation., *Environ. Sci.*
456 *Technol.*, 53(3), 1706–1714, 2019.
- 457 Faiola, C., Johansen, A. M., Rybka, S., Nieber, A., Thomas, C., Bryner, S., Johnston, J.,
458 Engelhard, M., Nachimuthu, P. and Owens, K. S.: Ultrafine particulate ferrous iron and
459 anthracene associations with mitochondrial dysfunction, *Aerosol Sci. Technol.*, 45(9), 1109–
460 1122, doi:10.1080/02786826.2011.581255, 2011.
- 461 Gao, Y.: Aeolian iron input to the ocean through precipitation scavenging: A modeling
462 perspective and its implication for natural iron fertilization in the ocean, *J. Geophys. Res.*,
463 108(D7), 4221, doi:10.1029/2002JD002420, 2003.
- 464 Goldstein, A., Robinson, A., Kroll, J., Drozd, G., Zhao, Y., Saliba, G., Saleh, R. and Presto, A.:
465 Investigating Semi-Volatile Organic Compound Emissions from Light-Duty Vehicles., 2017.
- 466 Hamad, S. H., Schauer, J. J., Antkiewicz, D. S., Shafer, M. M. and Kadhim, A. K. H.: ROS



- 467 production and gene expression in alveolar macrophages exposed to PM_{2.5} from Baghdad, Iraq:
468 Seasonal trends and impact of chemical composition, *Sci. Total Environ.*, 543, 739–745,
469 doi:10.1016/j.scitotenv.2015.11.065, 2016.
- 470 Hand, J. L., Mahowald, N. M., Chen, Y., Siefert, R. L., Luo, C., Subramaniam, A. and Fung, I.:
471 Estimates of atmospheric-processed soluble iron from observations and a global mineral aerosol
472 model: Biogeochemical implications, *J. Geophys. Res. D Atmos.*, 109(17), 1–21,
473 doi:10.1029/2004JD004574, 2004.
- 474 Haynes, J. P., Miller, K. E. and Majestic, B. J.: Investigation into Photoinduced Auto-Oxidation
475 of Polycyclic 2 Aromatic Hydrocarbons Resulting in Brown Carbon Production, *Environ. Sci.*
476 *Technol.*, 53(3), 10.1021/acs.est.8b05704, doi:10.1021/acs.est.8b05704, 2019.
- 477 Hickox, W. H., Werner, B. and Gaffney, P.: Air Resources Board, , (M1d), 1–6 [online]
478 Available from: http://www.arb.ca.gov/ei/see/memo_ag_emission_factors.pdf, 2000.
- 479 Hosseini, M. S. and Madarshahian, S.: Investigation of charge transfer complex formation
480 between Fe(III) and 2,6-Dihydroxy benzoic acid and its applications for spectrophotometric
481 determination of iron in aqueous media, *E-Journal Chem.*, 6(4), 985–992,
482 doi:10.1155/2009/417303, 2009.
- 483 Jickells, T. D., An, Z. S., Andersen, K. K., Baker, a R., Bergametti, G., Brooks, N., Cao, J. J.,
484 Boyd, P. W., Duce, R. a, Hunter, K. a, Kawahata, H., Kubilay, N., LaRoche, J., Liss, P. S.,
485 Mahowald, N., Prospero, J. M., Ridgwell, a J., Tegen, I. and Torres, R.: Global iron connections
486 between desert dust, ocean biogeochemistry, and climate., *Science*, 308(5718), 67–71,
487 doi:10.1126/science.1105959, 2005.
- 488 Kraemer, S. M.: Iron oxide dissolution and solubility in the presence of siderophores, *Aquat.*



- 489 Sci., 66(1), 3–18, doi:10.1007/s00027-003-0690-5, 2004.
- 490 Kraft, S., Stümpel, J. and Becker, P.: High resolution x-ray absorption spectroscopy with
491 absolute energy calibration for the determination of absorption edge energies, Rev. Sci.
492 Instrum., 67, 681, 1996.
- 493 Kuang, X. M., Scott, J. A., da Rocha, G. O., Betha, R., Price, D. J., Russell, L. M., Cocker, D. R.
494 and Paulson, S. E.: Hydroxyl radical formation and soluble trace metal content in particulate
495 matter from renewable diesel and ultra low sulfur diesel in at-sea operations of a research vessel,
496 Aerosol Sci. Technol., 51(2), 147–158, doi:10.1080/02786826.2016.1271938, 2017.
- 497 Lair, A., Ferronato, C., Chovelon, J. M. and Herrmann, J. M.: Naphthalene degradation in water
498 by heterogeneous photocatalysis: An investigation of the influence of inorganic anions, J.
499 Photochem. Photobiol. A Chem., 193(2–3), 193–203, doi:10.1016/j.jphotochem.2007.06.025,
500 2008.
- 501 Landreman, A. P., Shafer, M. M., Hemming, J. C., Hannigan, M. P. and Schauer, J. J.: A
502 Macrophage-Based Method for the Assessment of the Reactive Oxygen Species (ROS) Activity
503 of Atmospheric Particulate Matter (PM) and Application to Routine (Daily-24 h) Aerosol
504 Monitoring Studies, Aerosol Sci. Technol., 42(11), 946–957, doi:10.1080/02786820802363819,
505 2008.
- 506 Lawrence, S., Sokhi, R., Ravindra, K., Mao, H., Prain, H. D. and Bull, I. D.: Source
507 apportionment of traffic emissions of particulate matter using tunnel measurements, Atmos.
508 Environ., 77, 548–557, doi:10.1016/j.atmosenv.2013.03.040, 2013.
- 509 Ledakowicz, S., Miller, J. S. and Olejnik, D.: Oxidation of PAHs in water solutions by
510 ultraviolet radiation combined with hydrogen peroxide, Int. J. Photoenergy, 1(1), 1–6,



- 511 doi:10.1155/S1110662X99000100, 1999.
- 512 Lee, R. E. and Von Lehmden, D. J.: Trace metal pollution in the environment, *J. Air Pollut.*
513 *Control Assoc.*, 23(10), 853–857, doi:10.1080/00022470.1973.10469854, 1973.
- 514 Li, Y. and Xiang, R.: Particulate pollution in an underground car park in Wuhan, China,
515 *Particuology*, 11(1), 94–98, doi:10.1016/j.partic.2012.06.010, 2013.
- 516 Liati, A., Pandurangi, S. S., Boulouchos, K., Schreiber, D. and Arroyo Rojas Dasilva, Y.: Metal
517 nanoparticles in diesel exhaust derived by in-cylinder melting of detached engine fragments,
518 *Atmos. Environ.*, 101, 34–40, doi:10.1016/j.atmosenv.2014.11.014, 2015.
- 519 Lough, G. C., Schauer, J. J., Park, J. S., Shafer, M. M., Deminter, J. T. and Weinstein, J. P.:
520 Emissions of metals associated with motor vehicle roadways, *Environ. Sci. Technol.*, 39(3), 826–
521 836, doi:10.1021/es048715f, 2005.
- 522 Luo, C., Mahowald, N. M., Meskhidze, N., Chen, Y., Siefert, R. L., Baker, A. R. and Johansen,
523 A. M.: Estimation of iron solubility from observations and a global aerosol model, *J. Geophys.*
524 *Res. Atmos.*, 110(23), 1–23, doi:10.1029/2005JD006059, 2005.
- 525 Luo, C., Mahowald, N., Bond, T., Chuang, P. Y., Artaxo, P., Siefert, R., Chen, Y. and Schauer,
526 J.: Combustion iron distribution and deposition, *Global Biogeochem. Cycles*, 22,
527 doi:10.1029/2007GB002964, 2008.
- 528 Mackie, D. S., Boyd, P. W., Hunter, K. A. and McTainsh, G. H.: Simulating the cloud processing
529 of iron in Australian dust: pH and dust concentration, *Geophys. Res. Lett.*, 32(6), 1–4,
530 doi:10.1029/2004GL022122, 2005.
- 531 Majestic, B. J., Schauer, J. J. and Shafer, M. M.: Application of synchrotron radiation for



- 532 measurement of iron red-ox speciation in atmospherically processed aerosols, *Atmos. Chem.*
533 *Phys. Atmos. Chem. Phys.*, 7(Iii), 2475–2487, doi:10.5194/acpd-7-1357-2007, 2007.
- 534 Majestic, B. J., Anbar, A. D. and Herckes, P.: Elemental and iron isotopic composition of
535 aerosols collected in a parking structure, *Sci. Total Environ.*, 407(18), 5104–5109,
536 doi:10.1016/j.scitotenv.2009.05.053, 2009.
- 537 Marcus, M. A., Macdowell, A. A., Celestre, R., Manceau, A., Miller, T., Padmore, H. A. and
538 Sublett, R. E.: Beamline 10.3.2 at ALS: a hard X-ray microprobe for environmental and
539 materials sciences, *J. Synchrotron Radiat.*, 11, 239–247, doi:10.1107/S0909049504005837,
540 2004.
- 541 Marcus, M. A., Westphal, A. J. and Fakra, S. C.: Classification of Fe-bearing species from K-
542 edge XANES data using two-parameter correlation plots, *J. Synchrotron Radiat.*, 15(5), 463–
543 468, doi:10.1107/S0909049508018293, 2008.
- 544 May, A. A., Nguyen, N. T., Presto, A. A., Gordon, T. D., Lipsky, E. M., Karve, M., Gutierrez,
545 A., Robertson, W. H., Zhang, M., Brandow, C., Chang, O., Chen, S., Cicero-Fernandez, P.,
546 Dinkins, L., Fuentes, M., Huang, S. M., Ling, R., Long, J., Maddox, C., Massetti, J., McCauley,
547 E., Miguel, A., Na, K., Ong, R., Pang, Y., Rieger, P., Sax, T., Truong, T., Vo, T., Chattopadhyay,
548 S., Maldonado, H., Maricq, M. M. and Robinson, A. L.: Gas- and particle-phase primary
549 emissions from in-use, on-road gasoline and diesel vehicles, *Atmos. Environ.*, 88, 247–260,
550 doi:10.1016/j.atmosenv.2014.01.046, 2014.
- 551 Moore, J. K. and Abbott, M. R.: Surface chlorophyll concentrations in relation to the Antarctic
552 Polar Front: Seasonal and spatial patterns from satellite observations, *J. Mar. Syst.*, 37(1–3), 69–
553 86, doi:10.1016/S0924-7963(02)00196-3, 2002.



- 554 Neyens, E. and Baeyens, J.: A review of classic Fenton's peroxidation as an advanced oxidation
555 technique, *J. Hazard. Mater.*, 98(1–3), 33–50, doi:10.1016/S0304-3894(02)00282-0, 2003.
- 556 Norbeck, J. M., Durbin, T. D. and Truex, T. J.: Measurement of primary particulate matter
557 emissions from light-duty motor vehicles, Riverside., 1998.
- 558 Oakes, M., Weber, R. J., Lai, B., Russell, A. and Ingall, E. D.: Characterization of iron
559 speciation in urban and rural single particles using XANES spectroscopy and micro X-ray
560 fluorescence measurements: Investigating the relationship between speciation and fractional iron
561 solubility, *Atmos. Chem. Phys.*, 12(2), 745–756, doi:10.5194/acp-12-745-2012, 2012a.
- 562 Oakes, M., Ingall, E. D., Lai, B., Shafer, M. M., Hays, M. D., Liu, Z. G., Russell, A. G. and
563 Weber, R. J.: Iron solubility related to particle sulfur content in source emission and ambient fine
564 particles, *Environ. Sci. Technol.*, 46(12), 6637–6644, doi:10.1021/es300701c, 2012b.
- 565 Paris, R. and Desboeufs, K. V.: Effect of atmospheric organic complexation on iron-bearing dust
566 solubility, *Atmos. Chem. Phys.*, 13(9), 4895–4905, doi:10.5194/acp-13-4895-2013, 2013.
- 567 Paris, R., Desboeufs, K. V. and Journet, E.: Variability of dust iron solubility in atmospheric
568 waters: Investigation of the role of oxalate organic complexation, *Atmos. Environ.*, 45(36),
569 6510–6517, doi:10.1016/j.atmosenv.2011.08.068, 2011.
- 570 Park, S., Nam, H., Chung, N., Park, J.-D. and Lim, Y.: The role of iron in reactive oxygen
571 species generation from diesel exhaust particles, *Toxicol. Vitro.*, 20(6), 851–857,
572 doi:10.1016/j.tiv.2005.12.004, 2006.
- 573 Pehkonen, S. O., Siefert, R., Erel, Y., Webb, S. and Hoffmann, M. R.: Photoreduction of Iron
574 Oxyhydroxides in the Presence of Important Atmospheric Organic Compounds, *Environ. Sci.*



- 575 Technol., 27(10), 2056–2062, doi:10.1021/es00047a010, 1993.
- 576 Pignatello, J. J., Oliveros, E. and MacKay, A.: Advanced oxidation processes for organic
577 contaminant destruction based on the fenton reaction and related chemistry, Crit. Rev. Environ.
578 Sci. Technol., 36(1), 1–84, doi:10.1080/10643380500326564, 2006.
- 579 Rubio-Clemente, A., Torres-Palma, R. A. and Peñuela, G. A.: Removal of polycyclic aromatic
580 hydrocarbons in aqueous environment by chemical treatments: A review, Sci. Total Environ.,
581 478, 201–225, doi:10.1016/j.scitotenv.2013.12.126, 2014.
- 582 Saliba, G., Saleh, R., Zhao, Y., Presto, A. A., Lambe, A. T., Frodin, B., Sardar, S., Maldonado,
583 H., Maddox, C., May, A. A., Drozd, G. T., Goldstein, A. H., Russell, L. M., Hagen, F. and
584 Robinson, A. L.: Comparison of Gasoline Direct-Injection (GDI) and Port Fuel Injection (PFI)
585 Vehicle Emissions: Emission Certification Standards, Cold-Start, Secondary Organic Aerosol
586 Formation Potential, and Potential Climate Impacts, Environ. Sci. Technol., 51(11), 6542–6552,
587 doi:10.1021/acs.est.6b06509, 2017.
- 588 Santos, D. S. S., Korn, M. G. A., Guida, M. A. B., Santos, G. L. dos, Lemos, V. A. and Teixeira,
589 L. S. G.: Determination of copper, iron, lead and zinc in gasoline by sequential multi-element
590 flame atomic absorption spectrometry after solid phase extraction, J. Braz. Chem. Soc., 22(3),
591 552–557, doi:10.1590/S0103-50532011000300020, 2011.
- 592 Schauer, J. J., Kleeman, M. J., Cass, G. R. and Simoneit, B. R. T.: Measurement of emissions
593 from air pollution sources. 5. C1-C32 organic compounds from gasoline-powered motor
594 vehicles., Environ. Sci. Technol., 36(6), 1169–1180, doi:10.1021/es0108077, 2002.
- 595 Sedwick, P. N., Sholkovitz, E. R. and Church, T. M.: Impact of anthropogenic combustion
596 emissions on the fractional solubility of aerosol iron: Evidence from the Sargasso Sea,



- 597 Geochemistry, *Geophys. Geosystems*, 8(10), doi:10.1029/2007GC001586, 2007.
- 598 Shi, Z., Krom, M. D., Jickells, T. D., Bonneville, S., Carslaw, K. S., Mihalopoulos, N., Baker, A.
599 R. and Benning, L. G.: Impacts on iron solubility in the mineral dust by processes in the source
600 region and the atmosphere: A review, *Aeolian Res.*, 5, 21–42, doi:10.1016/j.aeolia.2012.03.001,
601 2012.
- 602 Sholkovitz, E. R., Sedwick, P. N. and Church, T. M.: Influence of anthropogenic combustion
603 emissions on the deposition of soluble aerosol iron to the ocean: Empirical estimates for island
604 sites in the North Atlantic, *Geochim. Cosmochim. Acta*, 73(14), 3981–4003,
605 doi:10.1016/j.gca.2009.04.029, 2009.
- 606 Sholkovitz, E. R., Sedwick, P. N., Church, T. M., Baker, A. R. and Powell, C. F.: Fractional
607 solubility of aerosol iron: Synthesis of a global-scale data set, *Geochim. Cosmochim. Acta*, 89,
608 173–189, doi:10.1016/j.gca.2012.04.022, 2012.
- 609 Stumm, W. and Morgan, J. J.: *Aquatic Chemistry: Chemical Equilibria and Rates in Natural*
610 *Waterse*, 3rd ed., Wiley-Interscience., 1996.
- 611 Tagliabue, A., Bowie, A. R., Philip, W., Buck, K. N., Johnson, K. S. and Saito, M. A.: Review
612 The integral role of iron in ocean biogeochemistry, *Nat. Publ. Gr.*, 543(7643), 51–59,
613 doi:10.1038/nature21058, 2017.
- 614 Teixeira, L. S. G., Rocha, R. B. S., Sobrinho, E. V., Guimarães, P. R. B., Pontes, L. A. M. and
615 Teixeira, J. S. R.: Simultaneous determination of copper and iron in automotive gasoline by X-
616 ray fluorescence after pre-concentration on cellulose paper, *Talanta*, 72(3), 1073–1076,
617 doi:10.1016/j.talanta.2006.12.042, 2007.



- 618 Verma, V., Fang, T., Guo, H., King, L., Bates, J. T., Peltier, R. E., Edgerton, E., Russell, A. G.
619 and Weber, R. J.: Reactive oxygen species associated with water-soluble PM_{2.5} in the
620 southeastern United States: Spatiotemporal trends and source apportionment, *Atmos. Chem.*
621 *Phys.*, 14(23), 12915–12930, doi:10.5194/acp-14-12915-2014, 2014.
- 622 Vile, G. F., Winterbourn, C. C. and Sutton, H. C.: Radical-driven fenton reactions: Studies with
623 paraquat, adriamycin, and anthraquinone 6-sulfonate and citrate, ATP, ADP, and pyrophosphate
624 iron chelates, *Arch. Biochem. Biophys.*, 259(2), 616–626, doi:10.1016/0003-9861(87)90528-5,
625 1987.
- 626 Wang, Y., Arellanes, C. and Paulson, S. E.: Hydrogen peroxide associated with ambient fine-
627 mode, diesel, and biodiesel aerosol particles in Southern California, *Aerosol Sci. Technol.*, 46(4),
628 394–402, doi:10.1080/02786826.2011.633582, 2012.
- 629 Zhao, Y., Nguyen, N. T., Presto, A. A., Hennigan, C. J., May, A. A. and Robinson, A. L.:
630 Intermediate Volatility Organic Compound Emissions from On-Road Diesel Vehicles: Chemical
631 Composition, Emission Factors, and Estimated Secondary Organic Aerosol Production, *Env. Sci.*
632 *Tech.*, 49, 11516–11526, doi:10.1021/acs.est.5b02841, 2015.
- 633 Zhao, Y., Nguyen, N. T., Presto, A. A., Hennigan, C. J., May, A. A. and Robinson, A. L.:
634 Intermediate Volatility Organic Compound Emissions from On-Road Gasoline Vehicles and
635 Small Off-Road Gasoline Engines., *Environ. Sci. Technol.*, 50, 4554–4563,
636 doi:10.1021/acs.est.5b06247, 2016.
- 637 Zhu, X., Prospero, J. M., Savoie, D. L., Millero, F. J., Zika, R. G. and Saltzman, E. S.:
638 Photoreduction of iron(III) in marine mineral aerosol solutions, *J. Geophys. Res. Atmos.*,
639 98(D5), 9039–9046, doi:10.1029/93JD00202, 1993.



640 **Tables and Figures and Captions**

641 Table 1: Average of total trace total and water soluble elements from car exhaust reported in EF
642 ($\mu\text{g kg-fuel}^{-1}$). These samples represent a range of different makes and models of cars. The
643 values in the parenthesis are the range of the vehicle populualtion. (n=32)

644 Table 2: Comparison of exhaust composition in g km^{-1} from different dynamometer studies
645 which included both gasoline and diesel powered light duty vehicles. The values are the mean of
646 the vehicle population and the values in the parenthesis are the minimum and maximum values.
647 This table is in g km^{-1} opposed to g kg-fuel^{-1} in Table 1.

648

649

650

651

652

653

654

655

656

657

658



659
660 Table 1:
661

	Total Elements	Water-Soluble Elements
Trace elements ($\mu\text{g kg-fuel}^{-1}$)		
Na	50 (0, 200)	30 (0, 100)
Mg	40 (0, 200)	8 (0, 60)
Al	100 (0, 2000)	20 (0, 100)
K	20 (0, 100)	20 (0, 100)
Ca	200 (0, 1000)	200 (0, 1000)
Ti	1 (0, 60)	0.2 (0, 2)
V	0.02 (0, 0.7)	0.02 (0, 0.7)
Cr	5 (0.04, 20)	0.6 (0, 4)
Mn	2 (0.02, 10)	1 (0.007, 8)
Fe	80 (0, 400)	20 (0, 200)
Co	0.2 (0, 1)	0.04 (0, 0.7)
Ni	5 (0, 30)	2 (0, 10)
Cu	20 (0, 200)	20 (0, 100)
Zn	60 (0, 300)	40 (0, 300)
As	0.006 (0, 0.03)	0.006 (0, 0.03)
Se	0.3 (0, 2)	0.05 (0, 0.5)
Rb	0.2 (0, 0.5)	0.01 (0, 0.1)
Sr	1 (0.01, 4)	0.6 (0.003, 3)
Mo	5 (0, 20)	3 (0.002, 30)
Rh	0.06 (0, 0.5)	0.007 (0, 0.1)
Pd	0.8 (0, 6)	0.3 (0, 4)
Ag	0.1 (0, 2)	0.03 (0, 0.5)
Cd	0.007 (0, 0.3)	0.009 (0, 0.05)
Sb	0.2 (0, 1)	0.1 (0, 0.9)
Cs	0.005 (0, 0.02)	0.002 (0, 0.02)
Ba	5 (0, 20)	3 (0.06, 20)
Ce	4 (0, 40)	0.4 (0, 2)
Pt	0.04 (0, 0.4)	0.01 (0, 0.2)
Pb	0.4 (0, 7)	0.3 (0, 7)
U	0.002 (0, 0.03)	0.002 (0, 0.03)

662

663

664

665



666

667

668 Table 2:

	This study Gasoline (n = 32)	Gasoline(Schauer et al., 2002) (n=9)	Gasoline(Norbeck et al., 1998) (n=40)	Diesel(Norbeck et al., 1998) (n=19)
Fleet Age	1990-2014	1981-1994	1972-1990	1977-1993
PM components (mg km⁻¹)				
OC	1 (0.06, 10)	3.3 ± 0.21	16 ± 32	150 ± 330
EC	10 (0.06, 100)	0.77 ± 0.023	3.5 ± 4.8	160 ± 100
sulfate	0.02 (0.001, 0.1)	0.08 ± 0.16	0.93 ± 1.9	0.77 ± .93
Trace elements (µg km⁻¹)				
Ag	0.01 (0, 0.25)	4.5 ± 20	0	0
Al	10 (0, 110)	20 ± 17	19 ± 37	31 ± 75
Ba	0.6 (0, 4.4)	0	0	68 ± 75
Ca	30 (0, 130)	26 ± 8.5	81 ± 120	650 ± 930
Cd	0.00 (0, 0.04)	0	0	0
Co	0.01 (0,0.25)	-	0	0
Cr	0.6 (0.008, 4)	0	0	6.2 ± 12
Cu	3 (0, 27)	0	6.2 ± 6.2	19 ± 31
Fe	10 (0, 62)	8.3 ± 2.3	280 ± 680	830 ± 1000
K	2 (0, 15)	3.0 ± 11.3	0	50 ± 170
Mg	7 (0, 120)	-	25 ± 31	99 ± 200
Mn	0.2 (0.002, 1.3)	0	0	6.2 ± 6.2
Mo	0.5 (0, 3.6)	2.3 ± 6.8	0	6.2 ± 12
Ni	0.6 (0, 5.2)	0	6.2 ± 12	12 ± 18
Pb	0.04 (0, 0.57)	0	25 ± 93	19 ± 62
Sb	0.02 (0, 0.21)	17 ± 39	0	0
Sr	0.1 (0, 0.68)	0.75 ± 2.3	0	0
Zn	7 (0, 37)	14 ± 1.5	110 ± 170	810 ± 1500

669

670

671

672